POLITECNICO
MILANO 1863

SCUOLA DI INGEGNERIA INDUSTRIALE
E DELL'INFORMAZIONE

Executive Summary of the Thesis

IMU-based upper limb kinematics: from exosuit control to motor primitives classification

Laurea Magistrale in Biomedical Engineering - Ingegneria Biomedica

Author: Carola Butera

Advisor: Prof. Emilia Ambrosini

Co-advisor: Eng. Elena Bardi

Academic year: 2022-2023

1. Introduction

1.1. Clinical problem

Upper limb (UL) motor impairment affects a significant number of individuals worldwide [1]. The need for assistance in carrying out activities of daily living (ADLs) can lead to a deterioration of the quality of life. Motor rehabilitation is therefore essential to mitigate the consequences of UL motor impairment. In-clinic rehabilitation consists in attending exercise and assessment sessions within the first six months after the occurrence of the compromising event. More in detail, the assessments are mostly based on standard clinical scales, among which the most popular are Fugl-meyer Assessment scale for Upper Extremity (FMA-UE) and Action Arm Research Test (ARAT). Despite their popularity, the application of these scales is time-consuming and can reduce the efficiency of the rehabilitative session. Moreover, evaluation inaccuracies can be introduced by ceiling effects, the subjective interpretation of the practitioner, and difficulties in recognizing compensatory strategies.
For these reasons, in recent years, wearable sensors have been proposed as tools for an objective assessment of UL recovery. These sensors can be used in the clinic but the application can also move to home environments. In this scenario they can be embedded, for example, in wearable robotic devices, to promote home-based therapy and to provide a continuous and reliable arm movement registration while performing the exercises. Indeed, the extension of the rehabilitation program over the 6-month period has proved to be effective [3]. However, limited resources in healthcare centers and the rising demand caused by population aging make it difficult to prolong the treatment in the clinic.

1.2. Machine learning for motor primitive classification

As mentioned, wearable sensors represent a promising tool to overcome the limitations of functional assessment clinical scales. Among the different possibilities, inertial measurement units (IMUs) can provide data on the acceleration, angular velocity, and orientation of the limb they are positioned on. To extract meaningful metrics from IMUs data, it is first necessary to segment the data stream into movements and motor primitives. Indeed, according to the taxonomy proposed by Schambra et al. [4], functional movements can be segmented into a sequence

of 'motion units', namely the primitives, which are characterized by a short duration and a precise goal. Machine-learning algorithms applied to IMUs data can be exploited to achieve this purpose.
For instance, Guerra et al. conducted a study aimed at the classification of rest, reach-to-grasp, release-to-retract primitives, and different subtypes of object manipulation [5]. The collection of data was performed on both healthy and stroke subjects by means of 7 IMUs placed on different upper body segments including hand and head. In particular, they exploited linear and angular acceleration, linear and angular velocity, position, and orientation provided by the sensors for the construction of a dataset characterized by 665 features. They used logistic regression and Hidden Markov models to classify data labeled through video observation, achieving an average precision of around 80%. Parnandi et al. [2] proposed an algorithm, based on deep neural networks, for the classification of 5 primitives: idle, stabilize, reach to grasp, reposition, and transport. They exploited kinematic data (77 features including 22 anatomical angles) obtained from 9 IMUs during the execution of typical rehabilitation exercises done while sitting and without trunk flexion. The proposed neural network architecture was based on sequence-to-sequence algorithms; in particular, they used Gated Recurrent Units (GRU). Their algorithm performed well in counting primitives, achieving an accuracy of around 90%. However, regarding the specific sensibility for each primitive, they obtained values from 67.7% to 82.2%. There is a gap in the literature regarding an application that specifically attempts to classify primitives in an uncontrolled scenario using joint angles.

1.3. Open challenges and scope of the thesis

In home-based rehabilitation and assistive scenarios, soft exoskeletons, known as exosuit, are gaining attention thanks to their lower weight, safety, and comfort. Exosuits, just like exoskeletons, are equipped with kinematic sensors to allow control. The present work is part of a wider project in which an upper limb cable-driven exosuit is being developed. The exosuit includes three IMUs that estimate the orientation of the arm of the user by means of rotation matrices.
The ultimate goal of this thesis is to assess UL movements of exosuit users during ALDs exploiting IMUs. The purpose of this assessment is to provide the input for the control system of the exosuit and to enable remote and continuous tracking of patients' progresses. This information may be used to provide feedback to the user so as to promote engagement.
More in detail, the first objective of this thesis concerns the development of an algorithm to extract upper limb 3D joint angles from IMUs: to control the anti-gravitational action of the exosuit, it is indeed necessary to know the 3D position of the arm in space. To this purpose, a calibration method needed to be implemented to compensate for misalignment between the sensor and the limb segments. Then, the algorithm to compute the 3D angles according to the International Society of Biomechanics (ISB) standard needed to be defined and validated against a robotic arm and an optoelectronic system.
The second objective of this work is the development of a classifier to perform automatic motor primitive classification on a dataset including simple and complex ADLs activities. The necessity to introduce motion classification arises considering that the final application of the exosuit will be in an uncontrolled environment and the evaluation of metrics has to be performed on meaningful windows of data. With the obtained upper limb kinematic model, which was derived from the previous objective, the main aim is to classify motor primities from activities of daily living by utilizing the joint angles as inputs.
This thesis focuses on these two objectives, leaving UL movement evaluation metrics for further work.

2. Materials and methods

2.1. IMU-based estimation of upper limb angles

This section describes the development and validation of a calibration method to align IMUs reference frames on body segments, and the formalization of a method to extract UL angles according to ISB convention. At this scope, NGIMU (x-io Technologies Limited Bristol, UK) sensors were used to acquire data at 150Hz for the validation on the robotic arm and at 50Hz for the one on humans. In particular, an IMU

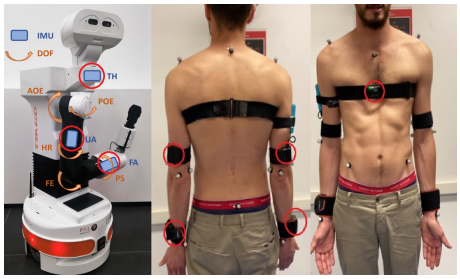

Figure 1: IMUs (circled in red) positioning on TIAGo robot (left) and healthy subject (right).

was positioned on the thorax, one on the upper arm, and on the forearm as in figure 1.
Validation was performed in 2 steps: comparing first IMU-based angle estimation with a robotic arm's (TIAGo, PAL Robotics Barcelona, Spain) encoders (sampling frequency of 35Hz), then on healthy participants comparing the validity of the measurements against an optoelectronic system (BTS SMART DX 400, BTS SPA, Italy) acquiring video at 100fps.

2.1.1 Calibration procedure

To avoid magnetic interference, the magnetometer of each IMU was switched off: this choice introduced the need to perform a reset of the sensor prior to each acquisition by aligning them to guarantee a common reference ground. The calibration procedure was based on the acquisition of two different poses: i)the N-pose and ii)the T-pose. During the N-pose, the user stands still with the arms resting and the palms of the hands pointing forward. In this configuration, the ISB joint angles are ideally null. The T-pose corresponds to a rotation of 90° of the arm on the coronal plane, but lower elevation angles were also accepted. This calibration aimed at defining the orientation of the upper arm (UA) and forearm (FA) with respect to the thorax (TH). This reference frame is characterized by a vertical y-axis, the x-axis pointing forward, and the z-axis to the right as depicted in Figure 2.

2.1.2 ISB angles computation

ISB defines the shoulder joint angles according to a Y-X-Y sequence of Euler angles rotations with respect to the reference frame in Figure 2. The first rotation around the Y axis defines the Plane Of Elevation angle (POE), the rotation around X the Angle Of Elevation (AOE), and the last rotation around the Y axis represents the Humeral Rotation (HR). The elbow joint is instead defined as a Z–X–Y rotation sequence. The first rotation around Z is the Flexion-Extension (FE) angle and the rotation around Y is the Pronation/Supination angle (PS). The rotation around X, which is descriptive of the ulnar deviation, will be considered as negligible. The orientation of the upper arm body segment (ISB,UA) with respect to the ground reference frame (G) can be defined as:

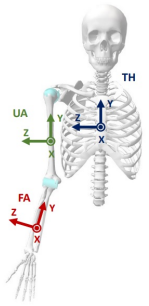

Figure 2: ISB reference frames. *TH* indicates the thorax, *FA* indicates the upper arm, *FA* indicates the forearm.

$$R^G_{UA} = R^G_{TH} R_y(\kappa POE) R_x(-\kappa AOE) R_y(\kappa HR) \quad (1)$$

where R^G_{TH} is the rotation matrix of the thorax body segment with respect to G and k is an index equal to 1 for the right arm, and -1 for the left arm. The rotation matrix describing the orientation of the forearm body segment with respect to G can be defined as:

$$R^G_{FA} = R^G_{UA} R_z(FE) R_y(\kappa PS) \quad (2)$$

The POE can be computed as:

$$POE = \angle(proj_{XZ_{TH}}(Y_{UA}), -\kappa Z_{TH}) \quad (3)$$

that is the relative angle between the projection of the y-axis of FA (Y_{UA}) onto the plane defined by the x-axis and the z-axis of TH(XZ_{TH}), and the z-axis of TH.
The AOE can be computed as:

$$AOE = \angle(Y_{UA}, Y_{TH}) \quad (4)$$

that is the relative angle between the y-axis of TH and the y-axis of UA.
Inverting Eq. (1) $R_y(HR)$ can be obtained, and HR can be computed as:

$$HR = tan^{-1}([R_y(HR)]_{1,3}, [R_y(HR)]_{1,1}) \quad (5)$$

where $[A]_{i,j}$ indicates the element of the matrix at the i-th row and j-th column.
FE can be computed as:

$$FE = \angle(Y_{FA}, Y_{UA}) \quad (6)$$

that is the relative angle between the y-axis of *FA* and the y-axis of FA.
Inverting Eq. (2) $R_y(PS)$ is defined, and *PS* can be computed as:

$$PS = tan^{-1}([R_y(PS)]_{1,3}, [Ry(PS)]_{1,1}) \quad (7)$$

Given that, because of soft tissues, there could be relative movement between the IMUs and the bones of the upper limb, the angle estimation could be corrupted. This is especially true for *HR* and *PS*. Therefore, an alternative definition of the *FA* rotation matrix, namely UA_{corr}, was proposed in order to define two variants for *PS* and *HR* angles.

$$X_{UA_{corr}} = (projY_{FAUA}Y_{UA}) - Y_{FA} \quad (8)$$

$$Y_{UA_{corr}} = Y_{UA} \quad (9)$$

$$Z_{UA_{corr}} = (X_{UA_{corr}}/|X_{UA_{corr}}|) \times Y_{UA_{corr}} \quad (10)$$

Where $projY_{FAUA}$ is the projection of y-axis of FA onto y-axis of *UA*. Finally, the variant of the *HR*, namely HR_{corr}, can be computed exactly like *HR* substituting in Eq. (1) *FA* with UAcorr. The same "corrected" *FA* rotation matrix was used to estimate an alternative *PS* angle, namely PS_{corr} starting from the application of UA_{corr} in Eq.(2).

2.1.3 Validation on the robotic arm

The experimental protocol for the validation of the IMU-based angle estimation against TIAGo's encoders was subdivided into 2 tests. During the first test, the IMUs were positioned trying to align the y-axis of the sensors with the robot's segments. The second test was instead conducted after positioning the IMUs in a non-aligned manner. Each test consisted in the execution of a sequence of movements that were registered both by TIAGo's encoders and IMUs. IMUs were positioned on TIAGo's upper arm, forearm, and head. Root Mean Squared Errors (RMSE) and correlation coefficients (r) of the two tests were evaluated and the mean percentage RMSE relative to the Range Of Motion (ROM) of every single angle (RMSE%) was computed.

2.1.4 Validation on healthy participants

A second validation was conducted on healthy participants by means of an optoelectronic system. 5 volunteers (mean age=24, 2 males, 3 females) were included in the acquisition protocol. 17 markers were positioned on bony landmarks of the thorax, upper arm, and forearm as suggested in [6]. The IMUs were positioned as in Figure 1. The acquisition protocol consisted of 5 simple tasks, aimed at exploring one single joint at the time. Drift control was performed and, if identified, the calibration procedure was repeated together with the task after which the drift was detected. To enable a comparison between the two measurement systems data were processed by interpolating the IMU signals at 100Hz to match the optoelectronic system sampling frequency, removing discontinuities, and removing the offset. Synchronization of signals was then performed by means of cross-correlation. Similar to the validation against TIAGo, mean value and Standard Deviation (SD) of RMSE, correlation coefficient, and RMSE% were computed among subjects.

2.2. Classification of motor primitives

2.2.1 Experimental setup and acquisition protocol

10 volunteers (1 male, 9 females, mean age=30.5, 3 left-handed, 7 right-handed) participated in the acquisition protocol. This consisted in the execution of a dataset including 8 'simple' ADLs (SADL) (moving a bottle, pouring water, drinking, answering the phone, mixing, reading a book, watering plants), and 3 'complex' ADLs (CADL) (breakfast preparation and eating, folding clothes, and personal hygiene routine). IMUs positioned as in Figure 2 were used for the registration of kinematic data of both arms. A GoPro HERO 5 (GoPro Inc.) was used to acquire videos to perform the labeling of the motor primitives (24 fps).

2.2.2 Ground truth identification and data preparation

In order to build a ground truth for the classification of motor primitives, a video labeling procedure was performed. At first, videos were cut so that the first frame coincided with the moment when a LED activation command was

sent to the IMU, indicating the acquisition's start. Frames were labeled according to the 5 primitives that had to be classified: 'idle', 'stabilize', 'reach', 'transport', and 'reposition'. A more refined data synchronization was then performed by minimizing the standard deviation of ISB angles during 'idle' and 'stabilize' movements. Each activity was zero-padded so that the length of activity in the dataset was homogeneous. In this way, by setting the batch size equal to the maximum exercise length, the neural network was allowed to process a whole exercise in a single iteration. Prior to the application to the neural network, labeled IMU data was segmented in overlapping (overlap=80%) 0.12 s windows. Train and test datasets were created by splitting each exercise into 80-20 % portions respectively.

2.2.3 Model architecture

The deep learning network was built as a sequence of layers. The model included a first a masking layer to assure that the algorithm ignored the null values added during zero-padding with an input shape equal to (6, 26), in which 6 is the window size, and 26 are the features corresponding to relative accelerations and angular velocities between segments, 7 ISB angles as computed in 2.1.2 and the angle between *TH* and *FA* y-axes. A Long-Short Term Memory (LSTM) layer and a dropout layer (dropout rate=0.5) were then added. The latter was introduced to prevent overfitting. Finally, a 'Dense' layer was stacked at the end of the model in order to map the inputs into a number of outputs equal to one of the possible labels by means of a 'softmax' activation function. The model was compiled using Adam optimizer and categorical cross-entropy as loss function.

2.2.4 Training and assessment of classification performance

The LSTM performance was tested for different values of hidden units, in particular, 50, 100, 200, and 300. Each model was trained 2 times for each hyperparameter choice: one using only SADL dataset both for training and testing (dataset A), the other using both SADL and CADL data for training and testing (dataset B). For each combination, 5 repetitions of training and testing were conducted by randomly choosing 5% of the training dataset for validation purposes.

3. Results and discussion

3.1. ISB angles: validation on the robotic arm

Results in terms of RMSE, RMSE% and correlation between the angles estimated from the IMUs and the motor encoders of TIAGo are presented in Table 1. As can be observed, signals from both tests show similar metrics. Moreover, both IMU signals are highly correlated to the one of TIAGo since they present a low RMSE and a high r. Correlation and RMSE values for *PS* and *FE* of Test 1 are slightly worse compared to Test 1, possibly due to inaccuracies introduced during calibration. The slightly worse RMSE that can be observed in the *POE*, can be traced back to the ill-posed definition of *POE* when *AOE* is equal or close to 0°.

3.2. ISB angles: Validation on healthy participants

Results in terms of RMSE and correlation between the angles estimated from the IMUs and the optoelectronic system are presented in Table 2 and Figure 3. These metrics were computed on signals after subtracting their mean values: for assessment purposes, is indeed more relevant to observe the ROM rather than the absolute angles.

Regarding the shoulder joint, the *AOE* presents higher errors compared to *POE* and HR_{corr} (RMSE<10°). This error can be introduced by calibration: during N-pose, in fact, the non-perfect alignment of upper arms to the vertical axis due to hips width could introduce an offset. HR_{corr} performed better than *HR*. The reason behind this might be that the latter was corrupted by the movements of the soft tissues around the humerus. HR_{corr} instead is computed from a rotation matrix that moves, theoretically, in unison with the bone.

Regarding the elbow joint, results are poor both for *FE*, *PS*, and PS_{corr}. The estimation of these angles, in fact, can be more easily biased by a drift, expected to cause an offset, or by a non-negligible ulnar deviation. Moreover, the value of the *FE* corresponding to zero may be different for the optoelectronic system and the IMUs: from Figure 3, in fact, is possible to notice that the

	Test 1			Test 2		
	r	RMSE [°]	RMSE[%]	r	RMSE [°]	RMSE[%]
POE	0.998	3.99	3.57	0.998	5.75	5.14
AOE	0.998	3.16	2.48	0.999	2.33	1.83
HR	0.999	3.23	2.67	0.999	2.27	1.87
FE	0.997	4.57	3.61	0.995	5.28	4.16
PS	0.997	2.54	2.41	0.993	7.37	6.99

Table 1: Correlation coefficient (r) and RMSE between TIAGO's encoders and IMU during two tests. RMSE% refers to the percentage of the RMSE with respect to the range of motion (ROM).

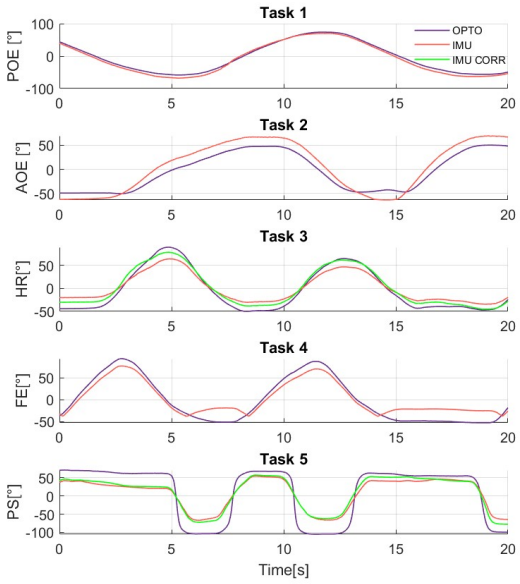

Figure 3: 'IMU'=angles acquired with IMU system (red), 'IMUcorr'=angles acquired with IMU system computed with *UA* correction (green), 'OPTO'=angles acquired with the optoelectronic system (blue).

FE estimated by the IMUs reverts its concavity for small angle values. The underestimation of *PS* and PS_{corr} by IMUs is probably due to the relative movement of the wristband and the more proximal position of *FA* sensor with respect to the wrist markers.

	RMSE[°]	RMSE%	r
POE	9,459 ±5, 270	6,525 ±3, 538	0,976 ±0, 028
AOE	16,000 ±4, 069	14,004 ±3, 674	0,952 ±0, 031
HR	15,365 ±3, 318	11,342 ±2, 373	0,963 ±0, 037
HR_{corr}	9,455 ±4, 380	7,303 ±3, 859	0,966 ±0, 032
FE	24,984 ±10, 932	16,397 ±7, 897	0,970 ±0, 019
PS	28,409 ±8, 239	16,905 ±3, 866	0,958 ±0, 022
PS_{corr}	29,654 ±12, 726	18,091 ±8, 802	0,919 ±0, 121

Table 2: Mean and standard deviation (SD) of RMSE, RMSE% evaluated on the range of motion (ROM) and correlation coefficients among 5 subjects.

	A	B
LSTM 50	0,738 ±0, 0058	0,700 ±0, 0033
LSTM 100	0,754 ±0, 0047	0,714 ±0, 0054
LSTM 200	0,765 ±0, 0062	0,711 ±0, 0046
LSTM 300	0,762 ±0, 0079	0,718 ±0, 0024

Table 3: Mean and SD values of f1-scores achieved by LSTM 50, 100, 200, and 300 during the testing phase of 2 combinations of datasets over 5 repetitions. 'A':training and testing only SADL data. 'B':training and testing SADL+CADL data.

During the validation process with optoelectronics, the results for human validation significantly deteriorate with respect to the one presented in 3.1. Several factors may have contributed to this degradation: the presence of soft tissues which is not compensated for *POE*, *FE*, and *AOE*, the calibration procedure, which can lead to some inaccuracies especially when the participant had a pronounced ulnar deviation, and the error introduced by the optoelectronic system itself given the lack of a standard protocol for UL kinematic assessment.

3.3. Classification of motor primitives

The acquisition process resulted in a dataset of $6 * 10^5$ windows. Results for different model complexity trained with different datasets (Table 3) show that dataset A achieved in general better performances with respect to dataset B, when more complex activities were classified. This result was predictable since in SADL dataset acquisition, the same activities were executed in the same way for all participants. On the contrary, some variability was introduced in the CADL tasks, in which subjects were able to move as they wished. For dataset B, the absolute f1-score slightly increases with LSTM layer depth: by increasing the model's complexity in fact, the algorithm could learn more complex representations. A performance deterioration can be

instead noticed in the case of dataset A: this suggests that increasing the complexity of the model could lead to overfitting.

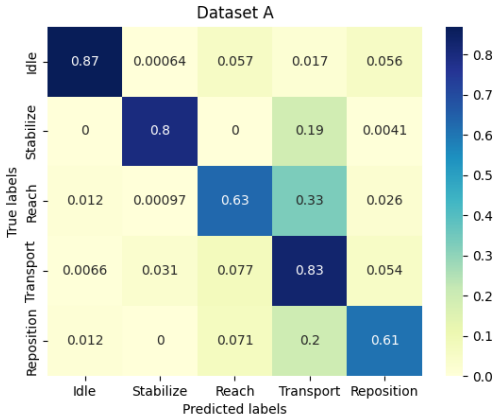

Figure 4: LSTM200 confusion matrix of dataset A.

From Figure 4 it is possible to notice that the primitives that were better classified were 'idle' and 'transport'. Datasets were, in fact, unbalanced, with a prevalence of 'transport' class compared to the others (50% of the entire dataset). The unbalancing of datasets had an effect on the prediction of 'reach' and 'reposition', which the algorithm still recognized as a movement but misclassified as 'transport'. However, even if 'idle' and 'stabilize' are characterized by very similar kinematics since the arm is practically stationary, is interesting to notice that they were clearly distinguished.

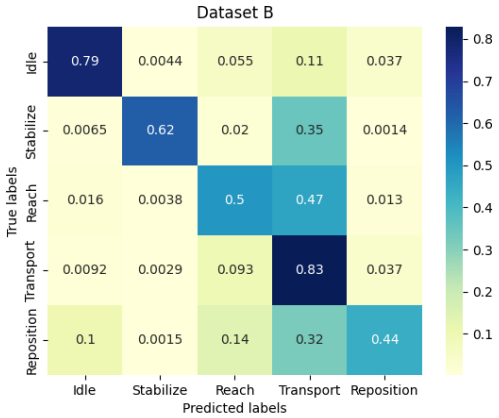

Figure 5: LSTM200 confusion matrix of dataset B.

As it is possible to observe in Figure 5, the unbalancing of the dataset had an effect also when the CADLs were introduced: the misclassification of 'reach' and 'reposition' is even more pronounced with respect to the previous model. This could be caused also by the fact that during CADLs, movements were faster and more varied compared to SADLs, and some errors may have been introduced due to inaccurate labeling.

4. Conclusions

The validation of ISB computation achieved excellent results in terms of correlation for the robotic arm. The validation on humans, as expected, in particular for *FE*, *AOE*, and *PS*, could be improved by introducing individual specific parameters such as ulnar deviation or hip width. Moreover, to improve IMUs' accuracy in the computation of ISB angles, future works should focus on drift compensation strategies. However, for classification purposes, is not necessary that the angles are estimated perfectly. The classification algorithm performed well in the recognition of the primitives that were more present in the dataset, even in the CADL scenario. Indeed, the misclassification of 'reach' and 'reposition' in 'transport' was consistent with their similar kinematic and the lack of information about hand movements. 'Stabilize' and 'idle' primitives, even if they are very similar in terms of arm kinematics, were well distinguished among the dataset A. It's reasonable to believe that, with a more balanced and wider dataset, the classification could perform much better. By the implementation of a clear computation method for ISB angles, and a simple neural network for primitive classification, this work represents a starting point for future developments for UL assessment in daily living scenarios.

References

[1] S. Chen and C. J. Winstein. A systematic review of voluntary arm recovery in hemiparetic stroke. *J. Neurol. Phys. Ther.*, 2009.

[2] A. Parnandi et al. PrimSeq: A deep learning-based pipeline to quantitate rehabilitation training. *PLOS Digit. Health.*, 2022.

[3] G. Kwakkel et al. Effects of augmented exercise therapy time after stroke. *Stroke*, 2004.

[4] H. M. Schambra et al. A taxonomy of functional upper extremity motion. *Front. Neurol.*, 2019.

[5] J. Guerra et al. Capture, learning, and classification of upper extremity movement primitives in healthy controls and stroke patients. *IEEE ICORR*, 2017.

[6] George Rab, Kyria Petuskey, and Anita Bagley. A method for determination of upper extremity kinematics. 2002.